Enhanced Microtubule Binding and Tubulin Assembly Properties of Conformationally Constrained Paclitaxel Derivatives †

ARTICLE *in* BIOCHEMISTRY · NOVEMBER 2007

Impact Factor: 3.02 · DOI: 10.1021/bi700753y · Source: PubMed

Enhanced Microtubule Binding and Tubulin Assembly Properties of Conformationally Constrained Paclitaxel Derivatives†

Natasha Shanker,‡ David G. I. Kingston,*,§ Thota Ganesh,§,|| Chao Yang,§ Ana A. Alcaraz,⊥ Matthew T. Geballe,⊥ Abhijit Banerjee,‡ Dennis McGee,# James P. Snyder,*,⊥ and Susan Bane*,‡

Department of Chemistry, Binghamton University, State University of New York, Binghamton, New York 13902, Department of Chemistry, M/C 0212, Virginia Polytechnic Institute and State University, Blacksburg, Virginia 24061, Department of Chemistry, Emory University, Atlanta, Georgia 30322, and Department of Biological Sciences, Binghamton University, State University of New York, Binghamton, New York 13902

Received April 20, 2007; Revised Manuscript Received July 22, 2007

ABSTRACT: Microtubule binding and tubulin assembly promotion by a series of conformationally restricted paclitaxel (PTX) derivatives was investigated. In these derivatives, the C-4 acetate of the taxane is tethered to the C-3′ phenyl at *ortho* and *meta* positions with different length linkers. The apparent affinity of these derivatives for GMPCPP-stabilized microtubules was assessed by a competition assay, and their influence on microtubule polymerization was evaluated by measuring the critical concentration of GDP-tubulin in the presence of the respective molecule. In general, taxane derivatives with higher apparent affinity for microtubules induced tubulin assembly more efficiently. Among the derivatives, molecules with the shortest tether display the strongest affinity for microtubules. These derivatives exhibited enhanced microtubule stabilization properties and efficiently induced GDP-tubulin assembly into microtubules at low temperature of 12 °C and in the absence of Mg^{2+} ions in 0.1 M PIPES. Based on molecular dynamics simulations, we propose that the enhanced ability to assemble microtubules by these taxane derivatives is linked to their ability to effectively shape the conformation of the M-loop of tubulin for cross-protofilament interaction.

Paclitaxel (PTX,[1] Taxol) and docetaxel (DTX, Taxotere) are clinically acclaimed chemotherapeutic agents widely used in the treatment of breast, lung, and ovarian carcinomas, and also for AIDS-related Kaposi's sarcoma (*1*−*4*). These congeners of the taxane family target the cellular microtubules by binding preferentially to polymeric tubulin and subsequently disrupting their dynamic assembly−disassembly properties (*5*−*8*). PTX was the first molecule discovered to assert this unique action of microtubule assembly promotion and stabilization (*5*). Since then several molecules that imitate the biological activity of PTX such as epothilones and discodermolide have been investigated and have moved into various stages of clinical development (*9*, *10*). Although taxanes are clinically successful chemotherapeutic drugs, poor aqueous solubility, complexities associated with their chemical synthesis, and induction of drug resistance produce clinical and industrial challenges with the current taxanes and provide impetus for preparing new generations of taxanes (*2*, *11*−*14*). The fundamental requirement for this task is to understand the molecular interactions between PTX and its receptor protein tubulin.

PTX is composed of a rigid hydrocarbon skeleton with appended side chains at carbons 2, 4, 10, and 13 (Figure 1). The side chain at C-13 is critical for the anticancer activity of the molecule. This portion of the molecule has considerable conformational flexibility and has been observed in 8−14 different conformations in solution (*15*, *16*).

Photoaffinity labeling studies established the binding site for PTX on the β-subunit of the tubulin heterodimer (*17*−*19*), and a clear picture of the binding site was achieved through electron crystallography of zinc induced tubulin sheets containing PTX (*20*−*22*). However, the tubulin bound conformation of PTX could not be ascertained due to the low resolution of the measurement. Subsequent refinement of the structure led to a proposed tubulin-bound conformation referred to as "T-Taxol" (*23*).

One approach to determine the bioactive conformation of the drug is to synthesize PTX derivatives in which the side chain has limited mobility and evaluate the ability of these molecules to interact with the PTX binding site on tubulin. Tethering the mobile C-13 side chain to another substituent

† This work was supported by NIH Grant No. CA-69571 (to D.G.I.K.) and NSF Grant No. DBI-0321046 (to D.M).

* To whom correspondence should be addressed. Phone: 607-777-2927. Fax: 607-777-4478. E-mail: sbane@binghamton.edu.

‡ Department of Chemistry, Binghamton University, State University of New York.

§ Virginia Polytechnic Institute and State University.

|| Current address: Department of Chemistry, Emory University, Atlanta, GA 30322.

⊥ Emory University.

Department of Biological Sciences, Binghamton University, State University of New York.

[1] Abbreviations: DAPI, 4′,6-diamidino-2-phenylindole dihydrochloride; DMSO, dimethyl sulfoxide; PTX, paclitaxel, Taxol; DTX, docetaxel, Taxotere; EDTA, ethylenediaminetetraacetic acid; EGTA, ethylene glycol-bis(2-aminoethylether)-*N*,*N*,*N*′,*N*′-tetraacetic acid; G-50, Spehadex G-50; GDP, guanosine 5′-diphosphate; GMPCPP, guanylyl-(α,β)-methylene-diphosphonate; GTP, guanosine 5′-triphosphate; $MgSO_4$, magnesium sulfate; N-AB-PT, 3′-*N*-*m*-aminobenzamido-3′-*N*-debenzamidopaclitaxel; PBS, 10 mM sodium phosphate buffer containing 0.9% sodium chloride (w/v), pH 7.2; PIPES, piperazine-1,4-bis(2-ethanesulfonic acid); PME, 0.1 M PIPES, 1 mM $MgSO_4$, and 2 mM EGTA, pH 6.90 at 25 °C.

10.1021/bi700753y CCC: $37.00
Published on Web 09/25/2007

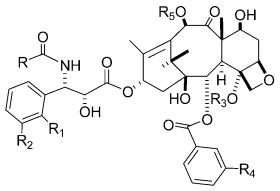

PTX, R: Ph R_1, R_2, R_4: H R_3: Ac R_5: Ac

DTX, R: t-BuO R_1, R_2, R_4: H R_3: Ac R_5: H

N-AB-PT, R: *m*-anilino R_1, R_2, R_4: H R_3: Ac R_5: Ac

Derivatives	R	$R_1 - R_3$	R_2	R_4	R_5
282	Ph	$(CH_2)_3CO$	H	H	Ac
258	Ph	*Z*-CH_2CH=CHCO	H	H	Ac
257	Ph	*E*-CH=$CHCH_2CO$	H	H	Ac
153	Ph	OCH_2CH=CHCO	H	H	Ac
289	Ph	$O(CH_2)_2CH$=CHCO	H	H	Ac
295	Ph	$O(CH_2)_4CO$	H	H	Ac
278	Ph	$O(CH_2)_5CO$	H	H	Ac
221	Ph	$O(CH_2)_6CO$	H	H	Ac
216	t-BuO	$(CH_2)_3CO$	H	H	Ac
234	t-BuO	$(CH_2)_3CO$	H	OCH_3	Ac
195	t-BuO	CH=$CHCH_2CO$	H	H	Ac
222	t-BuO	CH=$CHCH_2CO$	H	OCH_3	Ac

Derivatives	R	R_1	$R_2 - R_3$	R_4	R_5
283	Ph	H	$O(CH_2)_3CO$	H	Ac
220	Ph	H	CH=CH $(CH_2)_2CO$	H	Ac
214	Ph	H	OCH_2CH=$CH(CH_2)_2CO$	H	Ac

FIGURE 1: Structure of PTX and taxane derivatives.

in the molecule will restrict the possible conformations it can adopt, and by properly designing the features of the linkage, a molecule highly enriched in the T-Taxol conformer should be achievable. Such a conformationally restricted taxane can be expected to suffer a smaller entropic penalty in the receptor binding process and therefore experience a higher affinity for the binding site.

Recently, we prepared a number of PTX derivatives in which the C-3′ phenyl is tethered to the C-4 acetyl group. The synthetic strategy was pursued on the hypothesis that this cross-molecule linkage would cause target structures to adopt the bioactive conformation and lead to increased affinity for the taxane binding site on microtubules. In fact, some of the resulting compounds exhibit both higher cytotoxicity in PC3 and A2780 cell lines and increased potency as inducers of microtubule assembly in comparison with PTX (*24*, *25*). Neither of these assays, however, can directly test the original hypothesis concerning receptor site binding conformation. Polymerization assays are a function of both the intrinsic affinity of the taxane for its receptor site and the effect of ligand binding on assembly. The two are not necessarily related (*26*). Cytotoxicity will be affected by both these factors in addition to relative cell permeability, cytoplasmic metabolism, and other variables. Therefore, separate evaluations of the affinity of taxanes for microtubules and the efficacy of the bound ligand on microtubule assembly are necessary (*27*).

In this report, we measured the apparent affinities of conformationally restricted PTX derivatives for the PTX binding site on GMPCPP-stabilized microtubules and the effect of ligand binding on microtubule elongation, assessed by the critical concentration. In general, PTX derivatives that are more cytotoxic (*25*) show increased affinity for microtubules and enhanced ability to assemble GDP-tubulin into microtubules. Two of these molecules, however, are more potent promoters of tubulin assembly than would be predicted based on their apparent affinities for the PTX site on microtubules. In addition, these two molecules (**282** and **258**) are able to promote more robust assembly of GDP-tubulin into microtubules under conditions prohibitive to PTX-induced assembly. Molecular dynamics simulations suggest that the increased efficacy displayed by these two molecules may be due to induction of tubulin conformations that are more favorable for microtubule stabilization than the conformation induced by PTX.

MATERIALS AND METHODS

Protein and Ligand Preparation. Bovine brain tubulin was prepared by two cycles of temperature-dependent assembly−disassembly followed by ion exchange chromatography on phosphocellulose resin (*28*). Tubulin, free of microtubule-associated proteins, was stored in liquid nitrogen. Prior to use, tubulin was gently thawed and desalted into PME buffer by gel filtration in 1 mL columns packed with Sephadex G-50 pre-equilibrated in PME (*29*). The concentration of tubulin was determined spectrophotometrically at room temperature on a Hewlett-Packard model 8453 diode array spectrophotometer. The extinction coefficient employed for tubulin concentration determination was $\epsilon_{278nm,PME} = 1.23$ $(mg/mL)^{-1}$ cm^{-1} (*30*).

All chemicals used were of analytical grade and purchased from Sigma Chemicals unless specified. GMPCPP was synthesized by the method of Correia et al. (*31*). PTX, N-AB-PT, and the conformationally constrained taxane derivatives were synthesized as previously described (*24*, *25*, *32*). The stock solutions of 1 mM were made in DMSO for each ligand. The concentrations of taxanes and N-AB-PT were determined spectrophotometrically using extinction coefficients of $\epsilon_{273nm,DMSO} = 1.7 \times 10^3$ M^{-1} cm^{-1} for macrocyclic taxanes and $\epsilon_{320nm,DMSO} = 2.08 \times 10^3$ M^{-1} cm^{-1} for N-AB-PT (*26*, *32*).

Preparation of GDP-tubulin and GMPCPP-tubulin. GDP-tubulin and GMPCPP-tubulin with the E-site nucleotide fully replaced by GDP and GMPCPP, respectively, were prepared from GTP-tubulin as described previously (*32*, *33*). Unbound GDP and excess GMPCPP were not removed from the system.

Equilibrium Binding Competition between N-AB-PT and the Nonfluorescent PTX Derivatives. The relative affinities of PTX derivatives for stabilized microtubules were assessed by competition between the derivatives and fluorescent taxane, N-AB-PT. When excited at 320 nm, N-AB-PT fluoresces weakly in aqueous solution at 434 nm. However, in the presence of microtubules, an enhancement in fluorescence intensity as well as a blue spectral shift in the emission maximum of N-AB-PT is observed (*32*). The nonfluorescent PTX derivatives compete with N-AB-PT for the taxane binding site on microtubules. This results in a decrease of emission fluorescence intensity with increase in the concentration of nonfluorescent derivatives. The changes are useful for determination of apparent binding constants.

Tubulin bound to GMPCPP, a weakly hydrolyzable analogue of GTP, was used to form stabilized microtubules (*34*, *35*). To 5 μM of GMPCPP-microtubules in PME buffer, 5 μM N-AB-PT was added. The above solution was incubated with varying concentrations of nonfluorescent PTX derivatives (0−40 μM) at 37 °C for 30 min. The final

concentration of DMSO was maintained at 4% (v/v) in all cases. The fluorescence emission intensity for N-AB-PT bound to microtubules was measured at 413 nm upon excitation at 320 nm. Fluorescence emission spectra were recorded on a Jobin Yvon spectrofluorimeter. A 2 × 10 mm quartz cuvette employed for the measurements was oriented such that the excitation beam passed through the smaller path. The temperature was held constant at 37 °C with a circulating water bath. The apparent fluorescence of GMPCPP-microtubules due to light scattering was subtracted from the measurements. The maximum fluorescence emission intensity (F_0) was determined with 5 μM N-AB-PT and 5 μM GMPCPP-microtubules in the absence of taxane derivative. The fluorescence emission intensity (F) of the samples in the presence of taxane derivatives was recorded. From the plot of relative fluorescence intensity (F/F_0) against log of concentration of taxane derivative, an EC_{50} was obtained. This value is the concentration of taxane at which 50% of N-AB-PT is bound to microtubules, which was subsequently used to determine the apparent dissociation constant for the nonfluorescent taxane using the one site competition relation $K_i = EC_{50}/(1 + [\text{N-AB-PT}]/K_d)$, where K_i is the dissociation constant for nonfluorescent taxane; K_d is the dissociation constant for N-AB-PT with GMPCPP-microtubules {15 nM, (*32*)}; and [N-AB-PT] is 5 μM. The inverse of K_i is the apparent equilibrium binding constant K_a.

Critical Concentration Measurement. The critical concentration of GDP-tubulin in the presence of taxane derivatives in PME buffer was measured by the method of Andreu et al. (*26*). GDP-tubulin (2−10 μM) was polymerized with the analogues in a 1:1 molar ratio in PME buffer for 30 min at 37 °C. The polymerized GDP-tubulin was then distributed into 200 μL Beckman ultracentrifuge polycarbonate tubes. Microtubules were pelleted by centrifuging the samples in a Beckman Ti 42 rotor at 90000*g* for 1 h at 23 °C. The supernatant was carefully removed and separated from the pellet. Polymerized GDP-tubulin remained in the pellet, while the unpolymerized tubulin concentration in the supernatant was measured by absorption spectroscopy or by protein fluorescence (λ_{ex} = 290 nm, λ_{em} = 334 nm). The fluorescence emission was subtracted from that of the PME buffer and compared to a calibration plot of fluorescence emission intensity versus protein concentration. The concentration of unpolymerized tubulin in each sample is the critical concentration (*26*).

For the derivatives with weaker affinity than PTX for microtubules, a molar ratio of 4:1 of the ligand to GDP-tubulin was employed to ensure saturation of the ligand binding site.

Polymerization in the Absence of Mg^{2+} Ions. GDP-tubulin was prepared in 0.1 M PIPES, 1 mM EDTA buffer, pH 6.90. Assembly of GDP-tubulin into microtubules was monitored as increase in apparent absorption at 350 nm on the Hewlett-Packard spectrophotometer maintained at 37 °C. The polymerization was initiated by addition of the taxane to GDP-tubulin contained in thermally pre-equilibrated cuvettes.

Thermodynamic Analysis of Assembly. Tubulin assembly is characterized by a critical concentration, C_{cr}, below which no assembly of tubulin into microtubules is observed (*26*, *36*). The assembly is biphasic, typically involving a relatively slow nucleation step followed by a faster elongation phase. It has been shown that the apparent equilibrium constant (K_p) for the elongation phase is, to a good approximation, equal to the reciprocal of critical concentration, $K_p = C_{cr}^{-1}$ (*26*). Hence, the effect of a solution component on microtubule assembly can be determined by application of the Wyman theory of linked functions to the system: $\delta(\ln K_p)/\delta(\ln a_x) = \Delta\bar{\nu}_x$ (*26*, *37*). In the equation, a represents activity of solution component x, and the parameter $\Delta\bar{\nu}_x$ is the difference in the preferential interaction of x with tubulin in the monomer and polymer state.

The influence of Mg^{2+} ions on the elongation phase of taxane-induced GDP-tubulin assembly was determined from the Wyman plot. Critical concentrations of GDP-tubulin in the presence of **282** and PTX were determined in 0.1 M PIPES and 0.01 M phosphate buffer with varying Mg^{2+} ion concentration. The data are plotted against concentration of Mg^{2+} instead of ion activity (*36*).

Low Temperature Assembly Kinetics. The promotion of GDP-tubulin assembly in PME buffer at 12 °C by **282**, **258**, and **257** was monitored as the change in apparent absorption at 350 nm. The spectrophotometer was equipped with a temperature control water bath maintained at 12 °C.

Immunofluorescence Microscopy. A2780 and PC3 cells were grown on glass cover slips and fibronectin-coated glass cover slips, respectively, for 24 h and then treated with **282** or PTX for 24 h. Cells were then washed with PBS for 5 min; treated with methanol:acetone (1:1, v/v) for 10 min at 4 °C and then incubated with 20% normal goat serum for 10 min at room temperature. The cells were incubated with mouse monoclonal anti-α tubulin antibody (Zymed Technologies) for 1 h and with fluorescein isothiocyanate-conjugated-goat anti-mouse IgG (Jackson Immuno Research) for 45 min at 37 °C. The nucleus was stained with DAPI (0.1 μg/mL), and the cover slips were mounted on glass slides with Gel/Mount (Biomedia Corp., Cat. M01). In between each step, the cells were washed with PBS thrice. Photomicrographs were obtained using a Zeiss LSM 510 META confocal scanning laser microscope.

Electron Microscopy. Electron microscopy was performed to ascertain the morphology of polymerized GDP-tubulin. A drop of polymerized tubulin was placed on a carbon coated 200 mesh copper grid and negatively stained with 1% uranyl acetate. Electron micrographs were obtained using Hitachi 7000 TEM operated at 100 kV. Length distributions on the electron micrographs of microtubules were determined as previously described (*38*).

Molecular Dynamics of Ligands in Solution and Bound to α,β-Tubulin. Paclitaxel (PTX), **257**, **258**, and **282** structures were prepared as follows: PTX is an MMFF94s (*39*, *40*) optimized T-Taxol structure (*23*), while the **257** and **258** structures are the highest populated T-like conformers derived from NAMFIS analysis (*25*). Structure **282** was modeled saturating the bridge olefin in **257** and optimizing it with MMFF94s in Maestro (*41*). All four structures were docked into the 1JFF protein structure (*42*) using the default settings in the Glide module (*43*) of the Schrödinger software package (*41*). The protein structure was initially prepared and refined with the Protein Preparation tool in Glide, complemented with hydrogen atoms and optimized at side chain positions to avoid vdW contacts. The resulting RMSD for PTX (all atoms except hydrogens) between the 1JFF structure and the post-prep structure is 0.1 Å. The RMSD for the entire complex (all atoms except hydrogens) between the two is

0.2 Å, while the RMSD for PTX and a protein shell within 5 Å of the ligand is 0.2 Å. Following grid generation, extra precision (XP) flexible docking of the ligands was carried out. The vdW radii of the ligand atoms with partial atomic charges of less than 0.15 were scaled by 0.80, and the top 20 poses for each ligand were kept. For PTX, only the top pose maintained the T-Taxol shape, while the other 19 showed a variety of conformations and binding modes. Eleven of the twenty poses obtained for **257** were T-shaped, while the other nine positioned the C2-benzoyl side chain in different orientations. Only the top five poses for **258** were in the T-form; the rest covered a variety of binding modes that were up to 5 kcal/mol higher in energy. **282** resulted in 16 T-conformations. An additional four exhibited similar binding modes, but the C-13 benzamide or C-2 benzoyl groups were located in different positions. All twenty poses were no more than 2.5 kcal/mol higher in energy than the top pose. The resulting top T-pose for each ligand was employed for subsequent MD simulations.

All molecular dynamics (MD) simulations were performed with GROMACS 3.2.1 (*44*−*46*). The taxane ligand structures were prepared for the GROMOS96.1 force field (*47*) using the Dundee PRODRG2.5 Server (*46*). Each compound was solvated in a box of SPC water molecules (*48*): 512 for PTX and approximately 750 for the three bridged analogues. The systems ran for 1 ns, initially, to determine how they behaved and what changes in conformation could be detected. After minimal analysis, the systems were run for an additional 10 ns (11 ns total) at 300 K with a time step of 1 fs under NPT conditions (see below). Two plots were made to summarize the results of the dynamics. In the first, the RMSD of the molecules were calculated with respect to their starting T-form geometries (Figure S2, Supporting Information). The bridged analogues **258** and **282** remain in the T-form throughout the entire 11 ns simulation, although **257** experiences a conformational interconversion. The second plot (Figure 13) represents the RMS deviation of each atom in each molecule from its starting position throughout the entire simulation.

The structure of the α,*β*-tubulin dimer was converted to the GROMOS96 united atom force field (*47*); GTP, GDP, and the taxane ligands were parametrized with the PRODRG Server. The structures of apo-α,*β*-tubulin (GTP and GDP still present), PTX-bound α,*β*-tubulin (based on 1JFF) and **258**- and **282**-bound α,*β*-tubulin (based on the docking described above) were prepared for molecular dynamics simulation. Each α,*β*-tubulin-ligand complex was solvated in a box of 35,000 to 39,000 SPC water molecules (*48*) with two magnesium cations associated with the phosphates of the nucleotides and 36 sodium cations added to each system to neutralize the overall charge. After a steepest descents minimization, the systems were subjected to 20 ps restrained MD in which the water was allowed to equilibrate around and within the structures. The restraints were removed, and the system was simulated at 50 K for 5 ps to alleviate high energy interactions without large displacements. The systems were then treated with reverse annealing where the temperature was raised from 20 K to 300 K over a period of 25 ps. The simulations at 300 K were then allowed to run for over 5 ns. Apo and PTX-bound α,*β*-tubulin were simulated for 10 ns. Trajectories were analyzed and visualized using VMD (*49*). All simulations made use of PME electrostatics (*50*, *51*) with a 9 Å cutoff, were performed under NPT conditions utilizing the Berendsen thermostat (*52*), and employed a time step of 2 fs except during the 5 ps simulation at 50 K where a time step of 1 fs was adopted. All modeling figures were prepared using VMD (*67*) or PyMOL (*68*).

RESULTS

The premise for designing the macrocyclic taxanes (Figure 1) was restriction of the conformation of the PTX side chain to a limited set of conformers that would contain a sizable population of the "T-Taxol" conformation. Such a molecule would be anticipated to bind to the taxane site on tubulin with higher affinity than PTX. We have shown that a number of these macrocyclic taxanes are more cytotoxic and more potent inducers of *in vitro* tubulin assembly than PTX (*25*); however, these are not direct measurements of the association of the ligand with the receptor site. In this work, the relative affinity of the molecules for microtubules and the efficacy of the receptor-bound ligand were evaluated.

Association Constants. The apparent affinities of PTX and analogues for assembled tubulin were assessed by a competition assay. N-AB-PT is a fluorescent derivative of PTX that binds to the taxane site on microtubules with comparable affinity. Its binding is accompanied by a significant increase in quantum yield and a blue shift in the emission maximum (*32*). PTX and the analogues cause a concentration dependent decrease in N-AB-PT emission with GMPCPP-microtubules (Figure 2). These data were used to calculate the relative affinity of PTX and analogues for GMPCPP-microtubules as described under Materials and Methods.

Table 1 lists the values of the apparent affinity constants for binding of the taxanes to GMPCPP-microtubules at 37 °C. The derivatives with the C-4 acetate linked to an *ortho*-carbon of the C-3′ phenyl ring result in more stable complexes than *meta*-linked taxanes (apparent $\Delta\Delta G^\circ = 1.0-1.5$ kcal/mol). Among the *ortho*-linked derivatives, the relative affinity of the taxanes for GMPCPP-microtubules decreases with increasing number of atoms in the linker. Apparent association constants for molecules with 7−8 atom linkers could not be calculated due to the poor aqueous solubility of these ligands, which prevented the use of high enough concentrations to significantly inhibit N-AB-PT binding to microtubules (Figure 2, panel A). Analogues with a 5-atom (**295**) and a 6-atom linker (**278**) exhibit slightly greater and slightly reduced affinities, respectively, for GMPCPP-microtubules relative to PTX. Compounds with the shortest 3-atom tether (**257**, **258**, and **282)** (*25*) bind to GMPCPP-microtubules with a 2- to 3-fold greater apparent affinity than PTX. In part, the latter enhancement can be attributed to an entropic effect resulting from constraint of the drugs to a few conformations adopting the bioactive form, thereby enhancing an already favorable entropy change due to the burial of accessible surface area and the release of water.

Critical Concentration Measurements. The critical concentration of tubulin is the concentration below which no microtubule formation occurs. To a good approximation, it is the reciprocal of the elongation equilibrium constant, K_p, which is the measure of affinity of the end of a microtubule for the unassembled tubulin dimer (*36*). GDP-tubulin, in which the exchangeable GTP on *β*-tubulin has been replaced

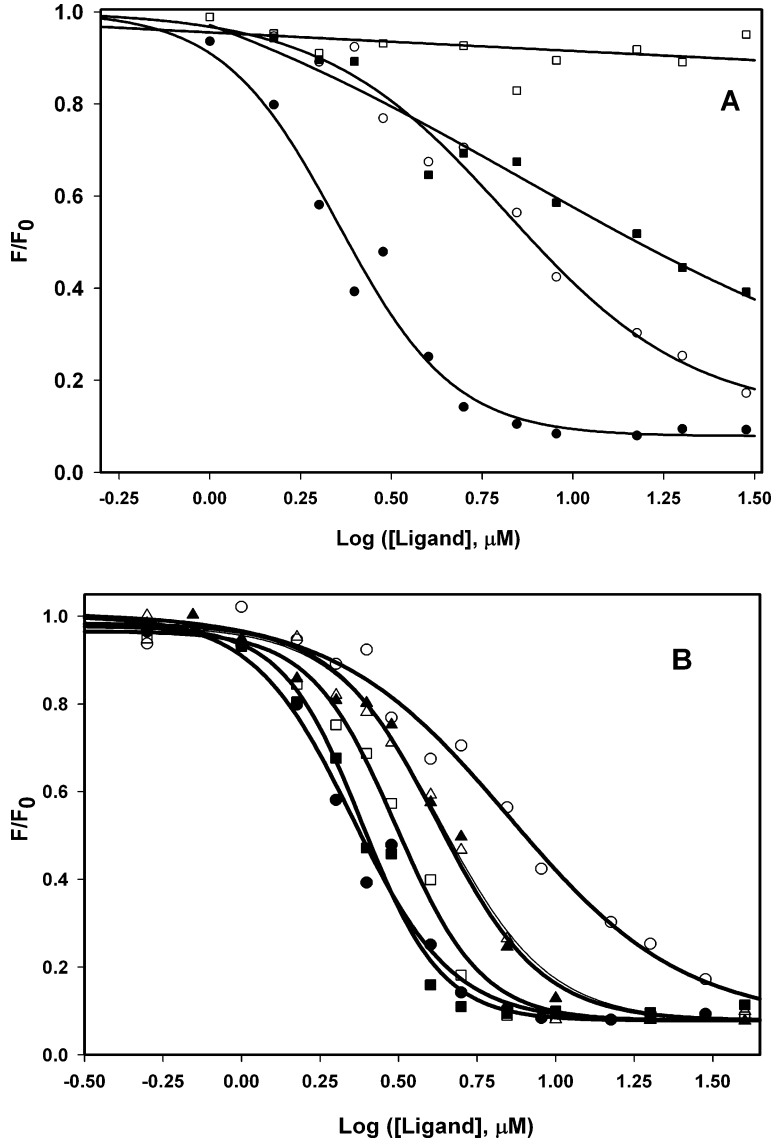

FIGURE 2: Competition between fluorescent N-AB-PT and macrocyclic taxane derivatives for PTX binding site on GMPCPP-microtubules. The experiments were performed at 37 °C as described under Materials and Methods. Relative fluorescence intensity of N-AB-PT (5 μM) bound to GMPCPP-microtubules (5 μM) in the presence of varying concentrations of taxanes (0−40 μM) is plotted against logarithm of the ligand concentration. A. **282** (●), PTX (○), **289** (■) and **221** (□). B. **282** (●), PTX (○), **216** (■), **234** (□), **195** (▲), **222** (△).

with GDP, does not assemble into microtubules in the absence of taxane under typical assay conditions (*26*, *37*, *38*). The critical concentration of GDP-tubulin in the presence of PTX is 3-fold greater than that of GTP-tubulin under the same experimental conditions (*37*, *38*). Since some of the compounds in this study are very potent inducers of tubulin assembly (*25*), it was necessary to use the less active form of the protein to get values for the critical concentration that could be measured with accuracy. The measurements were performed using centrifugation assay as described in Materials and Methods (Figure 3). These values are reported in Table 1.

The critical concentrations of GDP-tubulin with the *meta*-linked derivatives are about 3-fold higher than the critical concentration of GDP-tubulin with PTX (Table 1). In the *ortho*-linked derivative series, critical concentration increases with increasing chain length. The molecule **295** with a 5-atom tether induces a tubulin critical concentration similar to that induced by PTX. The 3-atom tethered compounds, **257** and **258**, decrease the critical concentration of GDP-tubulin by 2- to 4-fold compared to PTX. Thus, the taxanes with the shortest tether are most efficient in inducing GDP-tubulin assembly. The most notable is compound **282**, which exhibits an exceptionally high efficacy. The K_p for GDP-tubulin assembly in the presence of **282** is 12-fold greater than the K_p with PTX. In addition, the microtubules formed in the presence of equimolar concentrations of **282** and **258** were observed to be shorter than those formed in the presence of PTX. This was determined from the length distributions performed on the electron micrographs of the microtubules formed with the respective taxane (Figure 4). The "lag time" for tubulin assembly as observed by apparent light scattering appears to be significantly reduced in the presence of **258** and **282** in comparison to PTX-induced assembly (Figure 5). These observations suggest that the macrocyclic taxanes with the 3-atom tether result in more efficient tubulin nucleation than PTX.

Low-Temperature GDP-tubulin Assembly. Figure 6 illustrates that **282** promotes GDP-tubulin assembly at 12 °C; under the same conditions no significant assembly was

Table 1: Apparent Association Constants for Taxane Binding to GMPCPP-microtubules and Effect of Taxane Binding on GDP-tubulin Critical Concentration[a]

ligand	K_a ($\times 10^{-7}$ M)	$\Delta G°$ [b] (kcal/mol)	C_{cr} [c] (μM)	K_p [d] ($\times 10^{-5}$ M)	$\Delta G°$ [e] (kcal/mol)
PTX	5.1 ± 0.4	−10.90 ± 0.04	1.8 ± 0.2	5.5 ± 0.7	−8.16 ± 0.07
282	14.8 ± 0.5	−11.60 ± 0.02	0.15 ± 0.02	68.0 ± 10	−9.69 ± 0.09
258	12.2 ± 0.3	−11.50 ± 0.02	0.47 ± 0.06	21 ± 3	−8.97 ± 0.08
257	11.0 ± 0.3	−11.40 ± 0.01	0.89 ± 0.1	11 ± 1	−8.59 ± 0.07
295	7.0 ± 0.9	−11.10 ± 0.08	2.2 ± 0.5	4.5 ± 1	−8.0 ± 0.1
289	4.6 ± 2	−10.9 ± 0.3	3.4 ± 0.5	3.0 ± 0.4	−7.77 ± 0.08
153	3.2 ± 1	−10.6 ± 0.2	2.06 ± 0.07	4.8 ± 0.2	−8.06 ± 0.02
278	1.7 ± 0.1	−10.3 ± 0.2	3.1 ± 0.2	3.2 ± 0.2	−7.82 ± 0.04
221	>0.0100				
283	0.42 ± 0.04	−9.40 ± 0.05			
214	0.27 ± 0.04	−9.10 ± 0.09	4.5 ± 0.5	2.2 ± 0.2	−7.58 ± 0.06
220	0.14 ± 0.04	−8.7 ± 0.2	4.1 ± 0.2	2.5 ± 0.1	−7.65 ± 0.02
234	10.8 ± 0.4	−11.4 ± 0.02	0.5 ± 0.2	18 ± 5	−8.9 ± 0.2
216	13.8 ± 0.7	−11.5 ± 0.03	0.15 ± 0.05	68 ± 24	−9.7 ± 0.2
222	7.9 ± 0.3	−11.2 ± 0.02	1.5 ± 0.1	6.7 ± 0.6	−8.27 ± 0.09
195	7.7 ± 0.3	−11.2 ± 0.02	1.2 ± 0.2	8 ± 1	−8.4 ± 0.1

[a] All measurements were performed at 37 °C as described under Materials and Methods. [b] $\Delta G°$ is the apparent free energy change associated with binding of the ligand to GMPCPP-microtubules. [c] C_{cr} is the critical concentration of GDP-tubulin in the presence of the ligands. [d] K_p is the apparent elongation constant. [e] $\Delta G°$ is the apparent free energy change at steady state.

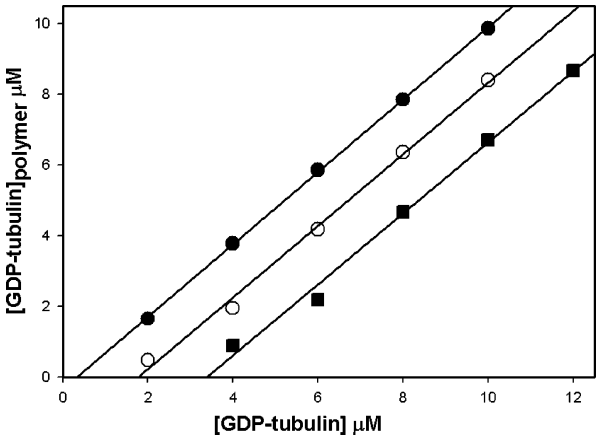

FIGURE 3: Critical concentrations of GDP-tubulin in the presence of taxane derivatives: **282** (●), PTX (○), and **289** (■) (molar ratio of GDP-tubulin to taxane is 1:1). GDP-tubulin was allowed to polymerize in the presence of taxane at 37 °C. Concentration of tubulin in the supernatant, after centrifugation at 90000*g*, was measured using fluorescence spectroscopy as described under Materials and Methods. Difference between the initial concentration of tubulin and that in the supernatant yielded the polymerized GDP-tubulin concentration.

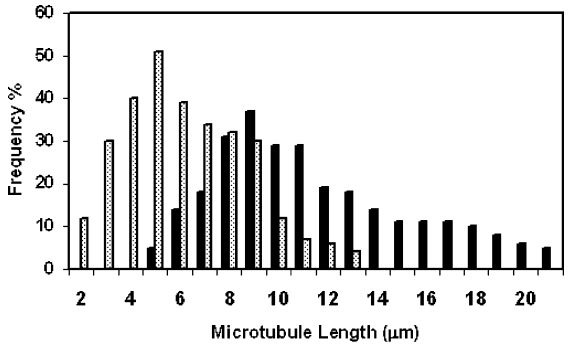

FIGURE 4: The length distribution of the microtubules formed in the presence of **258** (dotted cylinders) and PTX (solid cylinders). The lengths of the microtubules were measured from the electron micrographs (not shown).

observed in the presence of PTX. Critical concentrations for GDP-tubulin in the presence of 3-atom tethered macrocyclic taxanes and PTX were determined at 12 °C, 25 °C, and

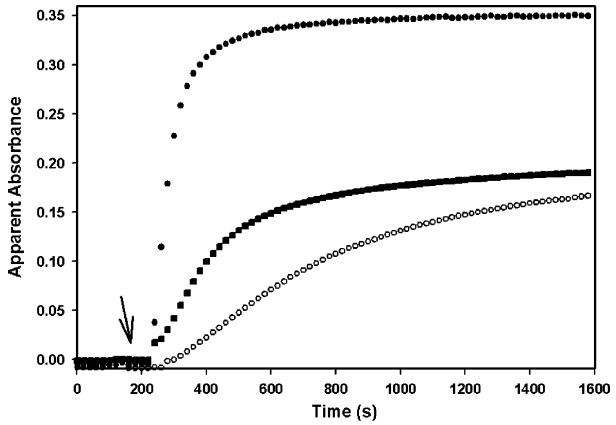

FIGURE 5: Assembly of GDP-tubulin monitored as increase in apparent absorbance at 350 nm measured at 25 °C in PME buffer in the presence of the following: **282** (●) 8 μM and 8 μM GDP-tubulin; **282** (■) 4 μM and 4 μM GDP-tubulin; PTX (○) 8 μM and 8 μM GDP-tubulin. (Arrow indicates the point of addition of the taxane.) **282**-induced GDP-tubulin assembly exhibits a smaller lag period and a greater extent of assembly in comparison to PTX.

37 °C (Table 2). As expected, the critical concentration of GDP-tubulin increases with a decrease in temperature. At 12 °C, **257**-induced GDP-tubulin assembly is similar to that of PTX. The critical concentration of GDP-tubulin in the presence of **257** was only 1.3-fold lower than PTX under these conditions. However, there is a 3-fold decrease in the critical concentration of GDP-tubulin relative to PTX in the presence of **258** or **282**.

One possible explanation for the different potencies is a temperature dependence of the apparent association constant, i.e., the affinity of PTX for microtubules may be affected by temperature to a greater extent than the affinity of the other ligands for microtubules. Therefore, the effect of the temperature change on the apparent affinity of PTX and **258** for GMPCPP-microtubules was evaluated in competition experiments (Figure 7). Changing the temperature may affect all components of the system, including the critical concentration for tubulin assembly and the affinity of N-AB-PT for microtubules. The goal of this experiment was not to quantitatively determine affinity constants at the lower temperature but to determine whether dropping the temper-

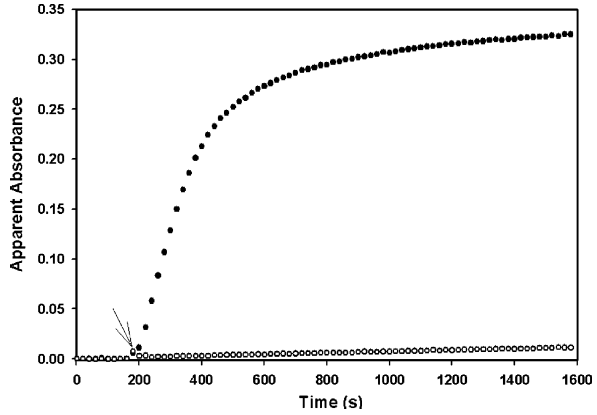

FIGURE 6: Assembly of 10 μM GDP-tubulin in PME buffer in the presence of 10 μM: **282** (●) and PTX (○) monotored as increase in apparent absorption at 350 nm. PTX fails to induce any significant polymerization at 12 °C. The ligand was added at the time indicated by the arrow.

Table 2: Effect of Temperature and Taxane on the Critical Concentration of GDP-tubulin

	C_{cr} (μM)		
ligand	12 °C	25 °C	37 °C
PTX	7.3 ± 0.4	3.6 ± 0.1	1.8 ± 0.2
282	2.0 ± 0.5	0.33 ± 0.06	0.15 ± 0.02
258	2.4 ± 0.2		0.47 ± 0.06
257	5.5 ± 0.6		0.9 ± 0.1

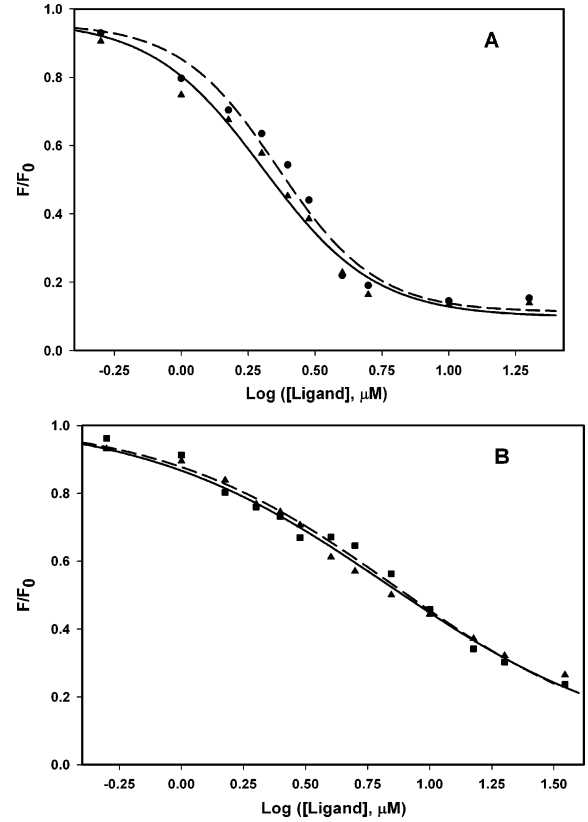

FIGURE 7: A. Competition of **258** with N-AB-PT for PTX site on GMPCPP-microtubules at 12 °C (●) and 36 °C (▲). B. Competition between N-AB-PT and PTX at 12 °C (■) and 36 °C (▲), respectively.

ature causes a differential change in apparent affinity of the two ligands for microtubules. It is seen in Figure 7 that the relative affinities are unchanged by the temperature difference. Therefore, the divergence in assembly promotion ability does not seem to be caused by a difference in ligand binding affinity.

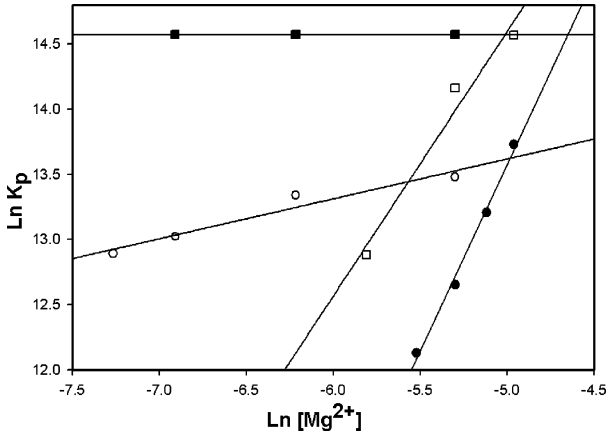

FIGURE 8: Wyman plots for **282** and PTX-induced GDP-tubulin assembly as a function of Mg^{2+} ion concentration. Critical concentrations of GDP-tubulin were measured in 0.01 M phosphate and 0.1 M PIPES, each containing 1 mM EDTA. In 0.01 M phosphate, measurements of critical concentrations were made at $MgCl_2$ concentrations (3 mM−7 mM), {PTX (●) and **282** (□)}. Critical concentrations of GDP-tubulin in 0.10 M PIPES, at varying $MgSO_4$ concentrations (1 mM, 2 mM, and 5 mM) {PTX (○) and **282** (■)}.

Influence of Mg^{2+} Ions on GDP-tubulin Assembly. The role of Mg^{2+} ions in taxane-induced tubulin assembly has been studied previously (*26*, *53*). An interesting observation for the 3-atom bridged taxanes **258** and **282** is their ability to successfully induce robust microtubule assembly in Mg^{2+} free, 0.1 M PIPES buffer. No assembly of GDP-tubulin with PTX was observed under identical conditions. To further investigate the role of Mg^{2+} ions in **282**-induced GDP-tubulin assembly, critical concentrations of GDP-tubulin with **282** were determined in 0.1 M PIPES at different Mg^{2+} ion concentrations (Figure 8). It is interesting to note that, for **282**, the critical concentration of GDP-tubulin remains unchanged within experimental error. The Wyman plot shows a straight line with a zero slope (Figure 8). This absence of Wyman linkage between the assembly elongation equilibrium constant, K_p, and Mg^{2+} ion concentration suggests that the taxane **282** is able to dispense the Mg^{2+} ion requirement for GDP-tubulin assembly in 0.1 M PIPES.

The generally observed inability of the taxanes to induce tubulin assembly in the absence of Mg^{2+} ions in 0.01 M phosphate buffer has been attributed to the lack of tubulin oligomers. The assembly state of GDP-tubulin under these solution conditions was directly assessed, but no comparable data exist for our usual buffer (0.1 M PIPES). We therefore repeated the experiments using 0.01 M phosphate buffer (Figure 8). Under these buffer conditions, both PTX and **282**-induced assembly require Mg^{2+}, indicating that tubulin oligomers are necessary for **282**-induced GDP-tubulin polymerization. A difference in the Mg^{2+} requirement for the two ligands is still observed in phosphate buffer. The slopes of the Wyman plots for **282** and PTX are 2.0 and 2.85, respectively, indicating that microtubules assembled with **282** incorporate one less Mg^{2+} per dimer than microtubules assembled with PTX. The difference in the slopes observed may suggest that the tubulin conformation induced by **282** differs from that induced by PTX.

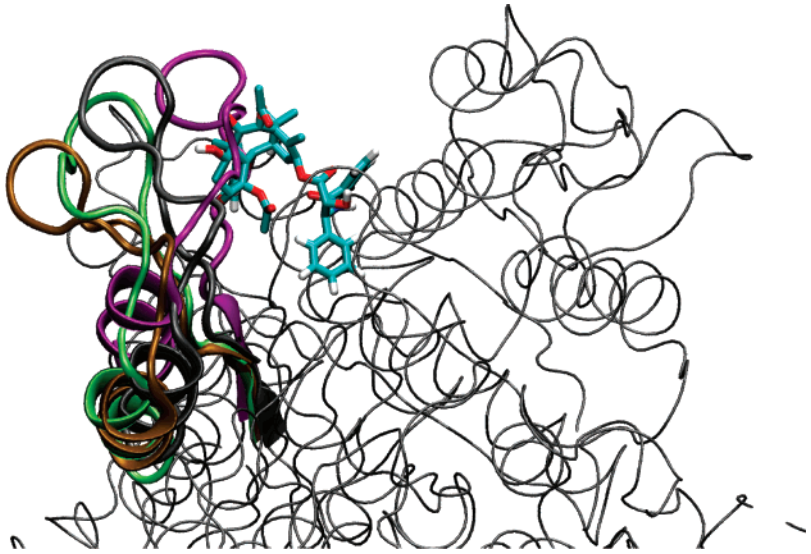

FIGURE 9: Four β-tubulin proteins overlapped following 4 ns molecular dynamics (MD) treatment at 300 K. M-loops at upper left; no ligand (purple); PTX (gray); **258** (green); **282** (brown). Paclitaxel is shown in the taxane binding site, the purple M-loop having moved in to fill the binding pocket.

Dynamic Effects of Bridged Taxanes on β-Tubulin. The individual complexes of PTX, **258**, and **282** with α,β-tubulin as well as the unliganded protein were prepared for computation, solvated, and subjected to molecular dynamics (MD) for at least 5 ns at 300 K with GROMACS as described under Materials and Methods. The key changes in the vicinity of the binding site are associated with the location and conformation of the M-loop. Figure 9 summarizes the results for the complexes at 4 ns, the time point at which each has equilibrated and achieved stability. To ensure that the latter were not arbitrarily chosen, average structures from the final 1 ns of simulation were generated and shown to mirror the structural features of the 4 ns complexes. The M-loop of the ligand-free protein depicted in purple collapses onto the taxane binding site, and in this conformation presumably blocks ligand binding. In the presence of PTX, however, the loop (gray, Figure 9) adopts a less compact conformation and serves as one of the boundaries for the taxane binding pocket. With **258** as ligand, the M-loop (green) recedes further, reaching its most modulated conformation (brown) when interacting with **282**. The full set of equilibrated complexes is portrayed in the Supporting Information (Figure S1). Seen from this dynamic point of view, both PTX and the bridged ligands have a dramatic but differential effect on the conformation of the M-loop. It is precisely those compounds exhibiting a 3-fold decrease in the critical concentration of GDP-tubulin relative to PTX and inducing significant microtubule assembly in Mg^{2+} free buffer (**258** and **282**) that are predicted to alter the M-loop conformation of β-tubulin to the greatest extent. In the following discussion, this point will be expanded and a structural basis for the effects outlined.

DISCUSSION

The initial hypothesis for this study was that restricting the conformations of the side chains of PTX by tethering the C-3′ phenyl to the C-4 acetyl group would result in an increased affinity for the taxane binding site on microtubules. In a previous report, we found that several taxane macrocycles were more cytotoxic and more potent inducers of microtubule assembly than PTX, which seemed to support the hypothesis (*25*). In the present study, we quantitatively determined the apparent association constants of the ligand/receptor interaction by competition experiments. Several conclusions can be drawn from these data. First, most of the hypotheses about interactions between the ligands and the receptor site that were based on cytotoxicity data hold true for receptor site binding. For example, the *meta*-linked compounds **283**, **214**, and **219** are 6−40-fold less cytotoxic than PTX, while the corresponding *ortho*-linked compounds (**153**, **295**, **278**) are similar to PTX in cytotoxicity and induction of tubulin assembly (*25*). The activity differences are reflected in the apparent association constants: the *meta*-linked molecules have an average affinity that is at least 10-fold less than that of the corresponding *ortho*-linked molecules.

The 3-atom tethered macrocycles are more cytotoxic than PTX. These derivatives (**257**, **258**, and **282**) also bind to microtubules with apparent affinities higher than PTX. *In vivo*, PTX and **282** both cause bundling of microtubules in PC3 and A2780 cells (Figure 10). The assembly of GDP-tubulin induced by these derivatives is more robust than that induced by PTX, as is evident from the low critical concentration values observed with these derivatives (Table 1) and their abilities to induce GDP-tubulin assembly in the absence of Mg^{2+} ions and at 12 °C.

The tremendously improved assembly promotion activity observed with the taxanes **257**, **258**, and **282** prompted us to investigate the impact of the 3-atom tether on other known taxanes that exhibit improved activity over PTX. For instance, the C-3′ amide substituent in DTX results in greater microtubule affinity and enhanced elongation constant than that of PTX-induced microtubules (*37*). Performing this substitution in a highly active macrocyclic taxane in our series, however, either had no effect on the affinity or efficacy of the ligand (compare **282** with **216**) or decreased both activities slightly (compare **257** with **195**) (Table 1). Similarly, it is known that certain substituents on the *meta*-position of C-2 benzoyl of PTX enhance microtubule assembly properties and increase the cytotoxicity (*54*−*56*).

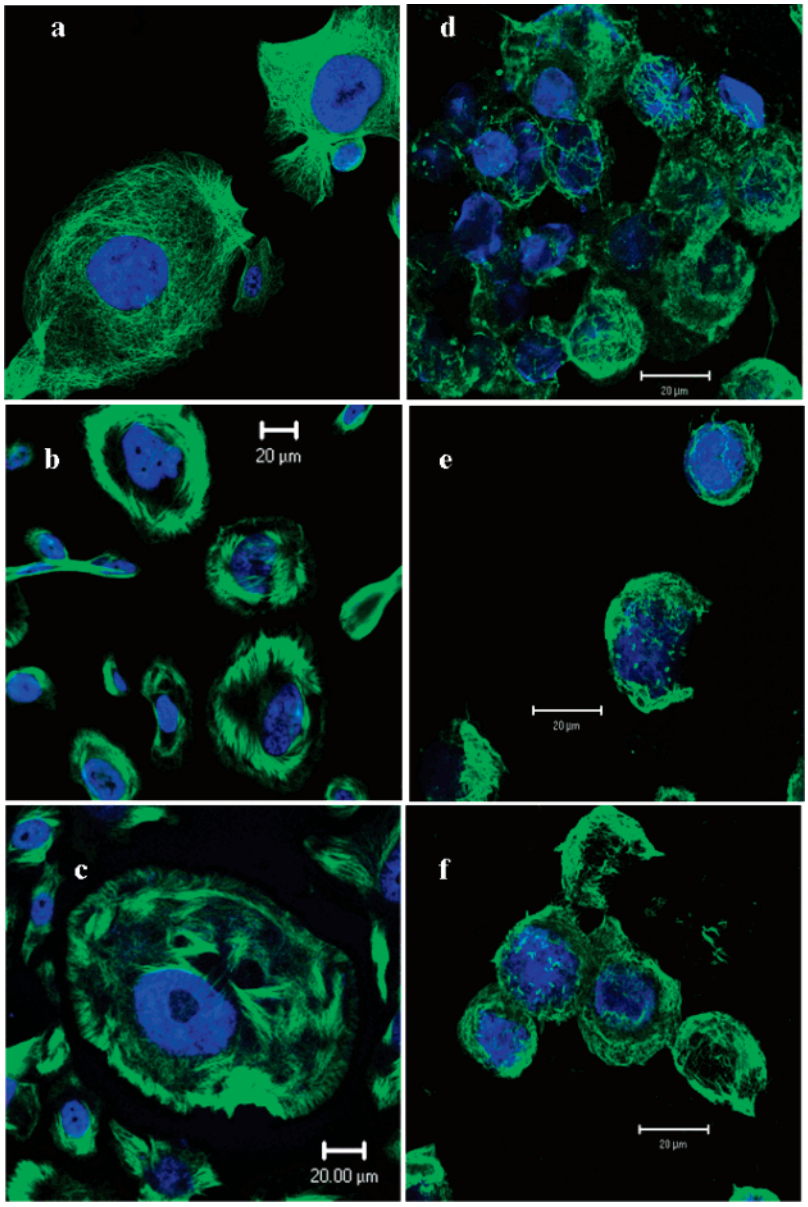

FIGURE 10: Immunofluorescence images of PC3 (a, b, c) and A2780 cells (d, e, f) after treatment with PTX and **282** for 24 h. PC3 cells: a, untreated; b, 2 μM PTX; c, 2 μM **282**. A2780 cells: d, untreated; e, 10 μM PTX; f, 10 μM **282**.

However, adding a methoxy group *meta* to the C-2 benzoyl produced essentially no effect on the association in these taxanes. These structural modifications in fact decrease the K_p values for three of the four ligands (**234**, **222**, and **195**). It therefore seems that, in this series, the structure of the macrocycle is a more important determinant of activity than substituents outside the ring.

Correlating Apparent Affinity with Efficacy. The data represented by Figure 11, derived from *ortho*-substituted C-3′ analogues (Figure 1), have been plotted as two separate trends. The dataset clustered about the solid trend-line represents a classic SAR in which protein affinity increases as a function of reduced bridge length, introduction of unsaturation, and the replacement of the C-3′ benzamido phenyl with O*t*Bu. The acyclic parent, PTX, clearly contributes to this correlation. At log $K_a \sim 8$, however, a second trend-line (dashed) materializes. At this point, the macrocyclic taxanes are more effective promoters of tubulin assembly than would be predicted based on their apparent affinities for microtubules. Compounds **282** and **258** are extreme in this respect, able to induce robust GDP-tubulin assembly at the low temperature of 12 °C and dispense with the Mg^{2+} ion requirement for tubulin assembly in 0.1 M PIPES. These bridged compounds, as well as **216** and **234**, are more highly tailored to forming stable microtubules than any other taxane studied to date. By contrast, PTX is unable to induce GDP-tubulin assembly under the same solution conditions, even when a 3-fold higher concentration of PTX is employed (data not shown).

A notable feature of the highly efficacious compounds is the steeper slope of the inhibition curves. The average slope of the sigmoidal curves for **216**, **282**, **234**, and **258** is 2.6 ± 0.4, which indicates that there is some cooperativity in ligand binding to the microtubules. In contrast, the average slope for compounds on the solid trend line in Figure 11 (**153**, **289**, **PTX**, and **295**) is 1.1 ± 0.3, so the association of these taxanes with microtubules can be properly described as an association of a ligand with identical and independent sites on the microtubule lattice. Cooperative ligand binding cannot be accurately described with the same analyses. The deviation

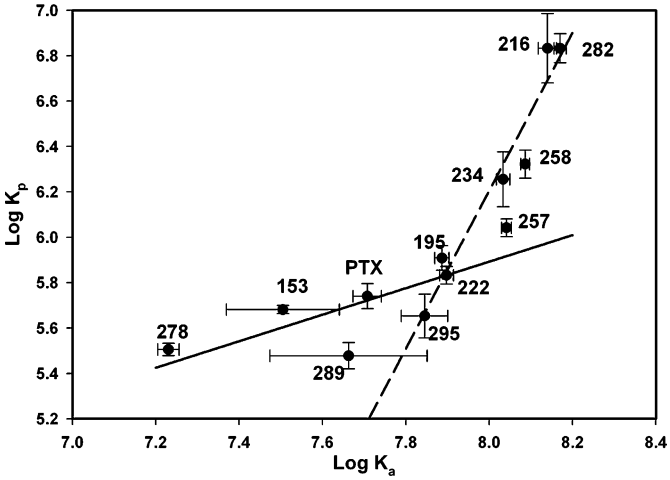

FIGURE 11: Correlation between ligand induced polymerization of GDP-tubulin (log K_p) and apparent affinity constant (log K_a) for the *ortho*-linked taxane derivatives. The relationship between affinity and efficacy changes when the size and flexibility of the C-3′ phenyl to C-4 acetate bridge are decreased. The lines illustrate the trends in the data.

from linearity for the K_a-K_p plot may be attributed to the presence of cooperativity in one set of ligands and the absence of cooperativity in others. Sorting out the various parameters involved in cooperative binding will require direct measurements of ligand binding to microtubules rather than competitition experiments (*57*). In the interim, the trends in the apparent affinity constant values reveal a fundamental difference in the ways that different classes of taxanes affect microtubule structure. In subsequent sections, we propose that the conformation adopted by β-tubulin when bound to **257**, **258**, and **282** is influenced by dynamic as well as static properties of the taxane analogues. In turn, this phenomenon appears to lead to more effective protofilament association and subsequent microtubule stability.

Fluctuations in Bridged Taxanes. While a great deal of effort has gone into defining the bioactive conformation and binding mode of paclitaxel and its analogues (*58*, *59*), the relative behavior of PTX, **258**, and **282** as depicted by Figure 9 and reflected by the SAR of Figure 11 suggests both static and dynamic aspects in the binding event rarely considered for ligands with such similar structures. A critical static element is registered by Figure 12a. In the latter, the α-carbon backbones of the taxane−tubulin complexes after 4 ns of MD were superposed and then the protein structure was hidden. The baccatin cores of the PTX, **258**, and **282** ligands occupy the same volume, but the C-2 benzoyl phenyl groups are displaced as shown by the red ellipse. It is noteworthy that the displacements are in the same direction as the M-loop translations of Figure 9. Measurement of the distances between C-4 and C-3′ in the individual taxanes (Figures 12b−d) reveals another parallel; namely, the distances increase in the order PTX < **258** < **282**, stretching the molecules along the approximate long axis. This static effect alone suggests that overall molecular length may reposition the taxane ligands in the binding site and promote M-loop transposition.

Overlaying the influence of ligand shape is a dynamic effect suggested by the MD behavior of the taxanes in the absence of protein. Figure S2 (Supporting Information) compares the overall RMSD for PTX, **257**, **258**, and **282** relative to T-Taxol in the electron crystallographic structure of PTX bound to β-tubulin over the 11 ns time course of the simulation. PTX assumes a number of conformations finding T-forms at least four times, while **257** samples at least two different conformations. By contrast, **258** and **282** are stable as T-Taxol conformers over the duration of their MD trajectories demonstrating a much reduced conformational flexibility. The latter is highlighted in terms of molecular fragments in Figure 13 by depicting the RMS fluctuation of each atom in the taxanes across the MD trajectories relative to the respective starting structures. PTX is most mobile with the C-4 acetate, the phenyl rings, and particularly the untethered C-3′ phenyl group exhibiting the largest fluctuations. While molecular flexibility falls in the order PTX, **257**, **258**, and **282**, the C-4 acetate and the C-3′ phenyl centers experience the greatest degree of motional damping from PTX/**257** to **258**/**282** (Figure 13) as expected for the termini of the short bridges connecting distal parts of the PTX framework.

Along this analogue series, two molecular features reinforce one another. That is, the greater the molecular flexibility (Figure 13), the more globular the taxane ligand (Figure 12). The least flexible structures are thus the more extended; namely, **258** and **282**. This observation correlates closely with the ability of these structures to enforce the greatest conformational change in the β-tubulin M-loop. The consequences for microtubule stabilization as reflected by maximal elongation constants, K_p, are discussed below.

Bridged Taxanes, the M-Loop, and K_p. As outlined above, the taxane series PTX, **257**, **258**, and **282** increases in molecular length (Figure 12), decreases in molecular mobility (Figure 13), and displaces the M-loop from its position in unliganded β-tubulin (Figure 9) in the order given. The operation of the ligands in the taxane binding cleft is best described by the panels of Figure 14, snapshots taken at the end of the protein ligand MD trajectories. Figure 14a shows that **282** resides near the luminal or interior surface of the microtubule. A 90° rotation of the protein (Figure 14b) illustrates that **282** spans the space between helix 1 (H1, at left in red) and the M-loop (at right in red). As pictured dramatically by the space-filling model in Figure 14c, the benzamido phenyl is pushed up against H1, while the C-2 phenyl ring is pinioned against the M-loop. This tight packing of the benzamido phenyl against H1 is facilitated by hydrogen bonds between Asp26 in β-tubulin and both the benzamido NH and 2′-hydroxyl hydrogens. A similar hydrogen bond between the benzamido NH and the backbone of helix H1 was observed for **258**, but not for PTX. It should be recalled that **282** is the most rigid bridged T-taxane that forces the MD-positioned M-loop furthest from the body of the protein (Figure 9). This contrasts with the more flexible PTX which binds in the more compact T-Taxol form. Also sandwiched between H1 and the M-loop, PTX sits somewhat deeper in the pocket and is less "right-shifted" toward the loop. The less pronounced molecular translation is partly the result of the conformational mobility of the unbridged molecule which is able to place its C-2 phenyl group in a narrow subpocket orthogonal to the disposition of the β-tubulin M-loop (Figure 14d). As a consequence, this loop is folded around the paclitaxel B, C, and D rings rather than being oriented outward toward the adjacent protofilament.

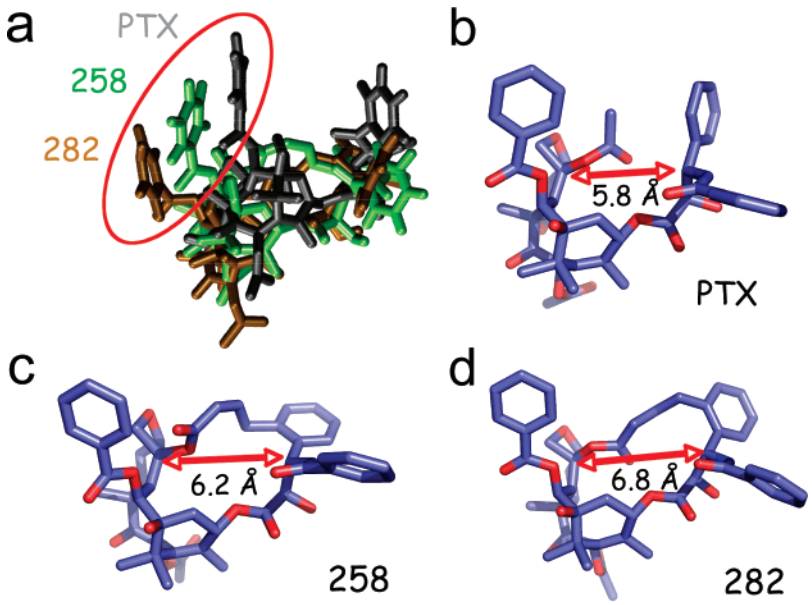

FIGURE 12: Geometric characteristics of PTX and bridged taxanes docked in β-tubulin and subjected to molecular dynamics. (a) Relative orientation of C-2 benzoyl phenyl groups following superposition of the protein complexes depicted in Figure 9. (b) Distance between C-4 and C-13 in PTX. (c) The expanded C-4 to C-13 distance in bridged **258**. (c) Maximal C-4 to C-13 distance achieved by **282**.

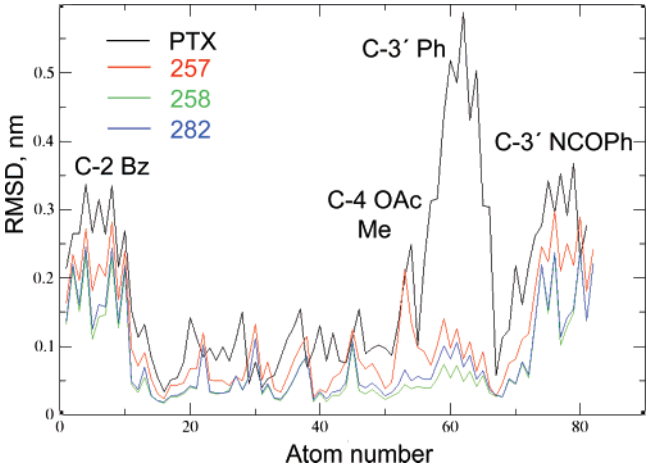

FIGURE 13: Relative atom fluctuations following molecular dynamics for PTX and three bridged taxanes in a box of water at 300 K for 11 ns. Movements are plotted as the average RMSD from atomic positions in the optimized geometries of the individual molecules; important functional groups are identified; PTX (black), **257** (red), **258** (green), **282** (blue).

The latter underpins the remarkable observation that the cytotoxicity of certain bridged taxanes is dominated by microtubule elongation (K_p) rather than apparent affinity (K_a, Figure 11). It is well-known that protofilament−protofilament interactions in microtubules are mediated by M-loops in contact with H1-S2 (the N-loop) and H2-S3 loops in a β-tubulin subunit within an adjacent protofilament (*22*, *60*) as modeled in Figure 15. It has also been suggested that PTX's microtubule stabilizing effect is likely to involve reshaping of the M-loop to induce a conformation that favors productive protofilament interaction (*22*, *23*, *61*). In order to achieve strong lateral contact, the M-loop needs to be extended away from the β-tubulin subunit and into the space between protofilaments. In order to maintain this contact, a restraint on conformational refolding of the M-loop would be ideal. We suggest that the rigid structures of compounds **258** and **282** serve this purpose by directing the M-loop toward the adjacent protofilament and by hindering both the loop's mobility and the establishment of a pool of rapidly equilibrating conformers. Depleting the latter conformational ensemble of forms that place the M-loop near the surface of the home β-subunit eliminates torsional isomers that cannot furnish productive lateral interactions. Compounds such as **258** and **282**, once docked into microtubules, act as rigid rods to hold the M-loop away from β-tubulin and further facilitate persistent contact with the secondary structure on the neighbor protofilament. The space-filling representation of the blue M-loop in Figure 15 illustrates this idea for bound but flexible PTX. We presume that structure **282** translates the M-loop slightly further into the inter-protofilament space, while offering the loop no opportunity to escape by conformational redistribution. In this way, the lateral interface is stabilized and microtubule depolymerization is suppressed.

Reshaping of the M-loop by the most potent bridged taxanes may reverberate through the microtubule lattice, allowing these taxanes to associate with microtubules in a cooperative manner. The idea that taxanes with similar structures can affect the architecture of microtubules in distinctly different ways is not unprecedented. PTX and DTX, which differ primarily in the substituent bonded to the C-3′ nitrogen (benzoyl and O*t*Bu, respectively), promote the formation of different microtubule lattices (*62*−*64*). Microtubules assembled in the presence of PTX have a significant population of 12-protofilament microtubules, while those assembled in the presence of DTX consist of mainly 13- and 14-protofilament microtubules, like those assembled in the presence of GTP. Microtubules assembled in the presence of DTX, however, can be reduced to 12-protofilament microtubules by addition of PTX to the solution (*65*). The exchange of ligand in the taxane binding site is accompanied by a reorganization of the microtubule without disassembly of the polymer. In a similar fashion, the tubulin conformation change caused by compounds such as **282** and **258** may affect the conformation of adjacent tubulin dimers, reshaping the lattice in a manner that favors taxane binding.

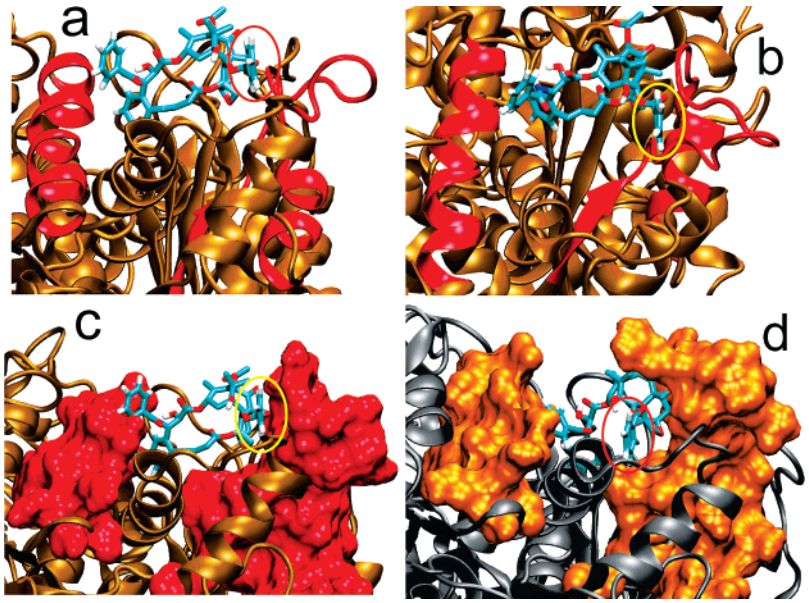

FIGURE 14: The binding sites of **282** and PTX in complex with β-tubulin following molecular dynamics at 300 K for 4 ns in a box of 35,000−39,000 water molecules. The C-2 benzoyl phenyl groups are identified within ellipses. (a) **282** sandwiched between H-1 and the M-loop and exposed to the microtubule lumen. (b) Rotation of the latter by 90° to show the tight van der Waals interaction between the C-2 phenyl and the M-loop. (c) Representation of H-1 and the M-loop as space-filling boundaries for **282** in the binding pocket. (d) PTX sequestered between H-1 and the M-loop shown in space-filling format.

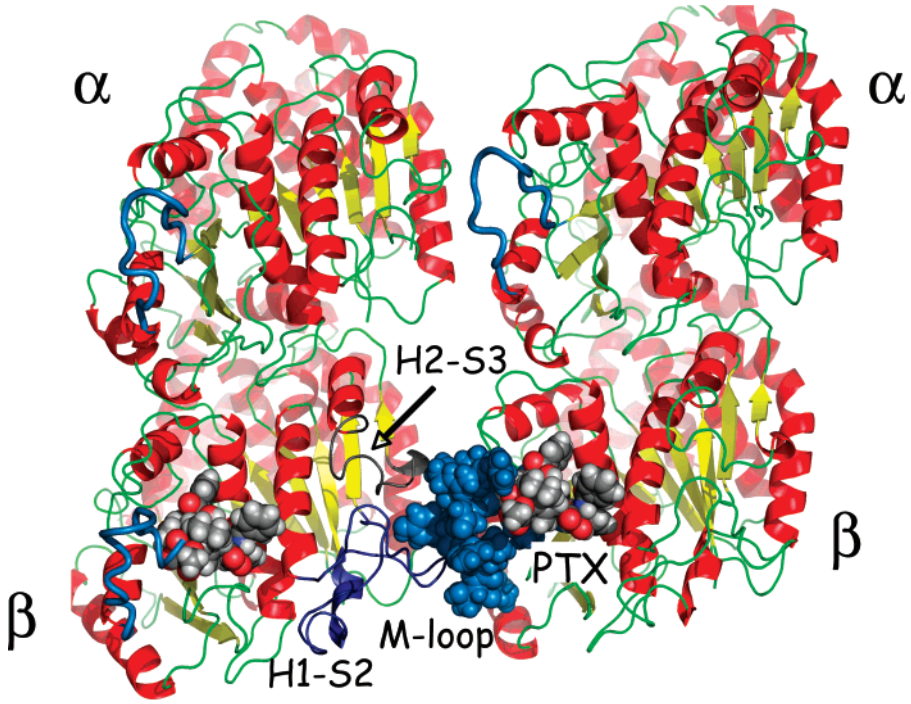

FIGURE 15: Four subunit component of a 13-protofilament microtubule illustrating the interaction between two vertically oriented protofilaments. In the β-subunits, two PTX molecules (space-filling) and two M-loops (blue) are highlighted. The space-filling M-loop associated with the β-subunit at lower right is in van der Waals contact with a PTX molecule to the right and the H1-S2 and H2-S3 loops to the left.

CONCLUSIONS AND FUTURE PROSPECTS

From the standpoint of microtubule assembly, taxanes synthetically bridged between the C-4 acetate methyl and the C-3′ phenyl groups fall into two classes. The first class contains *meta*-bridged and long-linked *ortho*-bridged molecules collected in Figure 1, as well as the multitude of untethered analogues prepared over the past 25 years, PTX and DTX among them (*66*). The compounds represented by this wealth of material exhibit significant conformational mobility particularly in the C-13 side chain, and the action of some of them can be traced to modest microtubule elongation capacity ($K_p < 10^6$) and affinities within a factor of 2 relative to PTX ($K_a < 10^8$, Table 1 and Figure 11). The second much smaller category encompasses four, maybe five relatively elongated taxanes (**216**, **234**, **257**, **258**, and **282**; Figure 1) characterized by the lack of significant dynamic behavior (Figure 13), little or no conformational freedom, high microtubule elongation constants ($K_p > 10^6$; Table 1

and Figures 11 and 12) and ostensible cooperative binding to microtubules. These same compounds are some of the most cytotoxic taxanes known with the ability to overcome taxane-resistant cell lines (*24*, *25*). We propose that the substances operate within the β-tubulin taxane binding site by holding the M-loop in an open orientation with a conformation that strengthens the contact between adjacent microtubule protofilaments to an extent unachievable with the more flexible PTX ligand. An important consequence of this proposal is the potential for designing other highly active analogues with reduced resistance profiles. Such molecules would seem to need to incorporate three characteristics: (1) molecular geometries able to precisely span the space between helix 1 and the M-loop (cf. Figure 14); (2) molecular rigidity to prevent the M-loop from folding out of the inter-protofilament regions; and (3) sufficient functionality to result in effective binding within the β-tubulin taxane cavity. Application of these ideas is under active pursuit in our laboratories.

ACKNOWLEDGMENT

The work was generously supported by NIH Grant CA-69571. We are thankful to Andrew Prussia (Emory University) for composing Figure 15.

SUPPORTING INFORMATION AVAILABLE

The equilibrated complexes of taxanes (PTX, **282**, and **258**) bound to β-tubulin and the overall RMSD for PTX, **257**, **258**, and **282** relative to T-Taxol over the 11 ns time course of the simulation. This material is available free of charge via the Internet at http://pubs.acs.org.

REFERENCES

1. Mekhail, T. M., and Markman, M. (2002) Paclitaxel in cancer therapy, *Expert Opin. Pharmacother. 3*, 755−766.
2. Zhao, J., Kim, J. E., Reed, E., and Li, Q. Q. (2005) Molecular mechanism of antitumor activity of taxanes in lung cancer, *Int. J. Oncol. 27*, 247−256.
3. Aversa, S. M., Cattelan, A. M., Salvagno, L., Crivellari, G., Banna, G., Trevenzoli, M., Chiarion-Sileni, V., and Monfardini, S. (2005) Treatments of AIDS-related Kaposi's sarcoma, *Crit. Rev. Oncol. Hematol. 53*, 253−265.
4. Salzberg, M., Thurlimann, B., Bonnefois, H., Fink, D., Rochlitz, C., von Moos, R., and Senn, H. (2005) Current Concepts of Treatment Strategies in Advanced or Recurrent Ovarian Cancer, *Oncology 68*, 293−298.
5. Schiff, P. B., Fant, J., and Horwitz, S. B. (1979) Promotion of microtubule assembly in vitro by taxol, *Nature 277*, 665−667.
6. Parness, J., and Horwitz, S. B. (1981) Taxol binds to polymerized tubulin in vitro, *J. Cell Biol. 91*, 479−487.
7. Horwitz, S. B. (1994) Taxol (paclitaxel): mechanisms of action, *Ann. Oncol. 5* (Suppl. 6), S3−S6.
8. Jordan, M. A., Wendell, K., Gardiner, S., Derry, W. B., Copp, H., and Wilson, L. (1996) Mitotic block induced in HeLa cells by low concentrations of paclitaxel (Taxol) results in abnormal mitotic exit and apoptotic cell death, *Cancer Res. 56*, 816−825.
9. Low, J. A., Wedam, S. B., Lee, J. J., Berman, A. W., Brufsky, A., Yang, S. X., Poruchynsky, M. S., Steinberg, S. M., Mannan, N., Fojo, T., and Swain, S. M. (2005) Phase II clinical trial of ixabepilone (BMS-247550), an epothilone B analog, in metastatic and locally advanced breast cancer, *J. Clin. Oncol. 23*, 2726−2734.
10. Mani, S., Macapinlac, M., Jr., Goel, S., Verdier-Pinard, D., Fojo, T., Rothenberg, M., and Colevas, D. (2004) The clinical development of new mitotic inhibitors that stabilize the microtubule, *Anticancer Drugs 15*, 553−558.
11. Gotaskie, G. E., and Andreassi, B. F. (1994) Paclitaxel: a new antimitotic chemotherapeutic agent, *Cancer Pract. 2*, 27−33.
12. Wilson, L., and Jordan, M. A. (2004) New microtubule/tubulin-targeted anticancer drugs and novel chemotherapeutic strategies, *J. Chemother. 16* (Suppl. 4), 83−85.
13. Jordan, M. A., and Wilson, L. (2004) Microtubules as a target for anticancer drugs, *Nat. Rev. Cancer 4*, 253−265.
14. Nuijen, B., Bouma, M., Schellens, J. H., and Beijnen, J. H. (2001) Progress in the development of alternative pharmaceutical formulations of taxanes, *Invest. New Drugs 19*, 143−153.
15. Ojima, I., Inoue, T., and Chakravarty, S. (1999) Enantiopure fluorine-containing taxoids: potent anticancer agents and versatile probes for biomedical problems, *J. Fluorine Chem. 97*, 3−10.
16. Snyder, J. P., Nevins, N., Cicero, D. O., and Jasen, J. (2000) The conformations of taxol in chloroform, *J. Am. Chem. Soc. 122*, 724−725.
17. Wu, Q., Bounaud, P. Y., Kuduk, S. D., Yang, C. P., Ojima, I., Horwitz, S. B., and Orr, G. A. (1998) Identification of the domains of photoincorporation of the 3′- and 7-benzophenone analogues of taxol in the carboxyl-terminal half of murine mdr1b P-glycoprotein, *Biochemistry 37*, 11272−11279.
18. Rao, S., He, L., Chakravarty, S., Ojima, I., Orr, G. A., and Horwitz, S. B. (1999) Characterization of the Taxol binding site on the microtubule. Identification of Arg(282) in beta-tubulin as the site of photoincorporation of a 7-benzophenone analogue of Taxol, *J. Biol. Chem. 274*, 37990−37994.
19. Rao, S., Orr, G. A., Chaudhary, A. G., Kingston, D. G., and Horwitz, S. B. (1995) Characterization of the taxol binding site on the microtubule. 2-(m-Azidobenzoyl)taxol photolabels a peptide (amino acids 217-231) of beta-tubulin, *J. Biol. Chem. 270*, 20235−20238.
20. Nogales, E., Wolf, S. G., Khan, I. A., Luduena, R. F., and Downing, K. H. (1995) Structure of tubulin at 6.5 A and location of the taxol-binding site, *Nature 375*, 424−427.
21. Nogales, E., Wolf, S. G., and Downing, K. H. (1998) Structure of the α, β- tubulin dimer by electron crystallography, *Nature 391*, 199−203.
22. Nogales, E., Whittaker, M., Milligan, R. A., and Downing, K. H. (1999) High-resolution model of the microtubule, *Cell 96*, 79−88.
23. Snyder, J. P., Nettles, J. H., Cornett, B., Downing, K. H., and Nogales, E. (2001) The binding conformation of Taxol in beta-tubulin: a model based on electron crystallographic density, *Proc. Natl. Acad. Sci. U.S.A. 98*, 5312−5316.
24. Ganesh, T., Guza, R. C., Bane, S., Ravindra, R., Shanker, N., Lakdawala, A. S., Snyder, J. P., and Kingston, D. G. (2004) The bioactive Taxol conformation on beta-tubulin: experimental evidence from highly active constrained analogs, *Proc. Natl. Acad. Sci. U.S.A. 101*, 10006−10011.
25. Ganesh, T., Yang, C., Norris, A., Bane, S. L., Ravindra, R., Banerjee, A., Metaferia, B., Thomas, A. L., Giannakakou, P., Alcaraz, A. A., Lakdawala, A. S., Snyder, J. P., and Kingston, D. G. I. (2007) Evaluation of the Tubulin-Bound Paclitaxel Conformation: Synthesis, Biology and SAR Studies of C-4 to C-3′ Bridged Paclitaxel Analogs, *J. Med. Chem. 50*, 713−725.
26. Diaz, J. F., Menendez, M., and Andreu, J. M. (1993) Thermodynamics of ligand-induced assembly of tubulin, *Biochemistry 32*, 10067−10077.
27. Diaz, J. F., Strobe, R., Engelborghs, Y., Souto, A. A., and Andreu, J. M. (2000) Molecular recognition of taxol by microtubules. Kinetics and thermodynamics of binding of fluorescent taxol derivatives to an exposed site, *J. Biol. Chem. 275*, 26265−26276.
28. Williams, R. C., Jr., and Lee, J. C. (1982) Preparation of tubulin from brain, *Methods Enzymol. 85* (Part B), 376−385.
29. Penefsky, H. S. (1979) Preparation of nucleotide-depleted F1 and binding of adenine nucleotides and analogs to the depleted enzyme, *Methods Enzymol. 55*, 377−380.
30. Detrich, H. W., 3rd, and Williams, R. C. (1978) Reversible dissociation of the α, β dimer of tubulin from bovine brain, *Biochemistry 17*, 3900−3907.
31. Vulevic, B., and Correia, J. J. (1997) Thermodynamic and structural analysis of microtubule assembly: the role of GTP hydrolysis, *Biophys. J. 72*, 1357−1375.
32. Li, Y., Edsall, R., Jr., Jagtap, P. G., Kingston, D. G., and Bane, S. (2000) Equilibrium studies of a fluorescent paclitaxel derivative binding to microtubules, *Biochemistry 39*, 616−623.
33. Seckler, R., Wu, G. M., and Timasheff, S. N. (1990) Interactions of tubulin with guanylyl-(beta-gamma-methylene)diphosphonate. Formation and assembly of a stoichiometric complex, *J. Biol. Chem. 265*, 7655−7661.

34. Muller-Reichert, T., Chretien, D., Severin, F., and Hyman, A. A. (1998) Structural changes at microtubule ends accompanying GTP hydrolysis: information from a slowly hydrolyzable analogue of GTP, guanylyl (α, *β*) methylenediphosphonate, *Proc. Natl. Acad. Sci. U.S.A. 95*, 3661−3666.
35. Hyman, A. A., Salser, S., Drechsel, D. N., Unwin, N., and Mitchison, T. J. (1992) Role of GTP hydrolysis in microtubule dynamics: information from a slowly hydrolyzable analogue, GMPCPP, *Mol. Biol. Cell 3*, 1155−1167.
36. Lee, J. C., and Timasheff, S. N. (1977) In vitro reconstitution of calf brain microtubules: effects of solution variables, *Biochemistry 16*, 1754−1764.
37. Diaz, J. F., and Andreu, J. M. (1993) Assembly of purified GDP-tubulin into microtubules induced by taxol and taxotere: reversibility, ligand stoichiometry, and competition, *Biochemistry 32*, 2747−2755.
38. Chatterjee, S. K., Barron, D. M., Vos, S., and Bane, S. (2001) Baccatin III induces assembly of purified tubulin into long microtubules, *Biochemistry 40*, 6964−6970.
39. Halgren, T. A., and Nachbar, R. B. (1996) Merck molecular force field .4. Conformational energies and geometries for MMFF94, *J. Comput. Chem. 17*, 587−615.
40. Halgren, T. A. (1999) MMFF VII. Characterization of MMFF94, MMFF94s, and other widely available force fields for conformational energies and for intermolecular-interaction energies and geometries, *J. Comput. Chem. 20*, 730−748.
41. *Maestro*, version 7.5 (2006) Schrodinger, LLC, New York.
42. Lowe, J., Li, H., Downing, K. H., and Nogales, E. (2001) Refined structure of α, *β*-tubulin at 3.5 A resolution, *J. Mol. Biol. 313*, 1045−1057.
43. *Glide*, version 4.0 (2005) Schrodinger, LLC, New York. http://www.schrodinger.com.
44. Lindahl, E., Hess, B., and Spoel, D. v. d. (2001) GROMACS 3.0: a package for molecular simulation and trajectory analysis, *J. Mol. Model. 7*, 306−317.
45. Schuttelkopf, A. W., and Aalten, D. M. F. v. (2004) PRODRG: a tool for high-throughput crystallography of protein-ligand complexes, *Acta Crystallogr., Sect. D: Biol. Crystallogr. 60*, 1355−1363.
46. At http://davapc1.bioch.dundee.ac.uk/cgi-bin/prodrg_beta.
47. van Gunsteren, W. F., Billeter, S. R., Eising, A. A., Hünenberger, P. H., Krüger, P., Mark, A. E., Scott, W. R. P., and Tironi, I. G. (1996) Biomolecular Simulations: The GROMOS96 manual and user guide, Vdf Hochschulverlag, ETH Zürich, Switzerland.
48. Hermans, J., Berendsen, H. J. C., Vangunsteren, W. F., and Postma, J. P. M. (1984) A Consistent Empirical Potential for Water-Protein Interactions, *Biopolymers 23*, 1513−1518.
49. Humphrey, W., Dalke, A., and Schulten, K. (1996) VMD: Visual molecular dynamics, *J. Mol. Graphics 14*, 33−38.
50. Darden, T., York, D., and Pedersen, L. (1993) Particle Mesh Ewald - an N.Log(N) Method for Ewald Sums in Large Systems, *J. Chem. Phys. 98*, 10089−10092.
51. Essmann, U., Perera, L., Berkowitz, M. L., Darden, T., Lee, H., and Pedersen, L. G. (1995) A Smooth Particle Mesh Ewald Method, *J. Chem. Phys. 103*, 8577−8593.
52. Berendsen, H. J. C., Postma, J. P. M., Vangunsteren, W. F., Dinola, A., and Haak, J. R. (1984) Molecular-Dynamics with Coupling to an External Bath, *J. Chem. Phys. 81*, 3684−3690.
53. Andreu, J. M., Garcia de Ancos, J., Starling, D., Hodgkinson, J. L., and Bordas, J. (1989) A synchrotron X-ray scattering characterization of purified tubulin and of its expansion induced by mild detergent binding, *Biochemistry 28*, 4036−4040.
54. Baloglu, E., Hoch, J. M., Chatterjee, S. K., Ravindra, R., Bane, S., and Kingston, D. G. (2003) Synthesis and biological evaluation of C-3′NH/C-10 and C-2/C-10 modified paclitaxel analogues, *Bioorg. Med. Chem. 11*, 1557−1568.
55. Kingston, D. G., Chaudhary, A. G., Chordia, M. D., Gharpure, M., Gunatilaka, A. A., Higgs, P. I., Rimoldi, J. M., Samala, L., Jagtap, P. G., Giannakakou, P., Jiang, Y. Q., Lin, C. M., Hamel, E., Long, B. H., Fairchild, C. R., and Johnston, K. A. (1998) Synthesis and biological evaluation of 2-acyl analogues of paclitaxel (Taxol), *J. Med. Chem. 41*, 3715−3726.
56. Grover, S., Rimoldi, J. M., Molinero, A. A., Chaudhary, A. G., Kingston, D. G., and Hamel, E. (1995) Differential effects of paclitaxel (Taxol) analogs modified at positions C-2, C-7, and C-3′ on tubulin polymerization and polymer stabilization: identification of a hyperactive paclitaxel derivative, *Biochemistry 34*, 3927−3934.
57. Sackett, D. L., and Saroff, H. A. (1996) The multiple origins of cooperativity in binding to multi-site lattices, *FEBS Lett. 397*, 1−6.
58. Kingston, D. G., Bane, S., and Snyder, J. P. (2005) The taxol pharmacophore and the T-taxol bridging principle, *Cell Cycle 4*, 279−289.
59. Jimenez-Barbero, J., Amat-Guerri, F., and Snyder, J. P. (2002) The solid state, solution and tubulin-bound conformations of agents that promote microtubule stabilization, *Curr. Med. Chem.: Anti-Cancer Agents 2*, 91−122.
60. Li, H. L., DeRosier, D. J., Nicholson, W. V., Nogales, E., and Downing, K. H. (2002) Microtubule structure at 8 angstrom Resolution, *Structure 10*, 1317−1328.
61. Amos, L. A., and Lowe, J. (1999) How Taxol stabilises microtubule structure, *Chem. Biol. 6*, R65−R69.
62. Andreu, J. M., Diaz, J. F., Gil, R., de Pereda, J. M., Garcia, de Lacobal, M., Peyrot, M., Briand, C., Towns-Andrewsll, E., and Bordas, J. (1994) Solution structure of taxotere-induced microtubules to 3-nm resolution. The change in protofilament number is linked to the binding of the taxol side chain, *J. Biol. Chem. 269*, 31785−31792.
63. Arnal, I., and Wade, R. H. (1995) How does taxol stabilize microtubules, *Curr. Biol. 5*, 900−908.
64. Meurer-Grob, P, Kasparian, J, Wade, RH. (2001) Microtubule structure at improved resolution, *Biochemistry 40*, 8000−8008.
65. Diaz, J. F., Valpuesta, J. M., Chacon, P., Diakun, G., and Andreu, J. M. (1998) Changes in microtubule protofilament number induced by Taxol binding to an easily accessible site. Internal microtubule dynamics, *J. Biol. Chem. 273*, 33803−33810.
66. Georg, G. I., Chen, T. T., Ojima, I., and Vyas, D. M., Eds.(1995) *Taxane anticancer agents: Basic science and current status*, ACS Symposium Series 583, pp 1−353, American Chemical Society, Washington, DC.
67. Humphrey, W., Dalke, A., and Schulten, K. (1996) VMD−Visual Molecular Dynamics, *J. Mol. Graphics, 14*, 33−38; http://www.ks.uiuc.edu/Research/vmd/.
68. DeLano, W. L. (2002) *The PyMOL Molecular Graphics System*, DeLano Scientific, Palo Alto, CA; http://www.pymol.org.

BI700753Y